Journal of Coastal Research	SI	88	61–76	Coconut Creek, Florida	2019

Short-term to Decadal-scale Sand Flat Morphodynamics and Sediment Balance of a Megatidal Bay: Insight from Multiple LiDAR Datasets

Franck Levoy[†], Edward J. Anthony[††], Job Dronkers[‡], Olivier Monfort[†*], and Anne-Lise Montreuil[§]

[†]Université de Caen Normandie-CREC
Luc-sur-Mer, France

[††]Aix Marseille Univ, CNRS, IRD
INRA, Coll France, CEREGE
Aix-en-Provence, France

[‡]Netherlands Centre of Coastal Research
Prinses Mariannelaan
Voorburg, The Netherlands

[§]Hydrology and Hydraulic Engineering, Vrije Universiteit Brussel
Brussels, Belgium

www.cerf-jcr.org

www.JCRonline.org

ABSTRACT

Levoy, F.; Anthony, E.J.; Dronkers, J.; Monfort, O., and Montreuil, A.-L., 2019. Short-term to decadal-scale sand flat morphodynamics and sediment balance of a megatidal bay: Insight from multiple LiDAR datasets. *In:* Castelle, B. and Chaumillon, E. (eds.), *Coastal Evolution under Climate Change along the Tropical Overseas and Temperate Metropolitan France. Journal of Coastal Research*, Special Issue No. 88, pp. 61–76. Coconut Creek (Florida), ISSN 0749-0208.

This study presents the results of LiDAR surveys, spanning 15 years (2002-2017), of the shallow inner sector of Mont-Saint-Michel Bay, a megatidal embayment in Normandy, France, and a UNESCO World Heritage site famous for its monastery. The objective of these surveys was to obtain a better understanding of the morphodynamic processes in this megatidal environment. The campaign has highlighted the circumstances and very short timescales at which changes occur in the channel configuration of the inner bay. It has also been demonstrated the high variability of sediment import and export, which involves not only the tide, but also wind speed and direction. Part of the variability is also related to fluctuations in river discharges into the bay. Since 2009, engineering works have been carried out in the bay. These are aimed at re-establishing the maritime character of the bay around the granite outcrop (Mont-Saint-Michel) on which was built the monastery, and which was increasingly subject to accretion. The main channel of the inner bay shifted recently to a more southward position than observed during the past decades. Yet, from the topographic LiDAR data up to May 2017, it is presently not possible to identify the influence of the engineering works on sedimentation processes beyond a limited zone around the Mont. However, the pursuit of LiDAR surveys is necessary in order to determine whether, in the course of the next decade, the North-South migrations of the Sée-Sélune channel induced by the 18.6 y nodal cycle are affected or not by these works.

ADDITIONAL INDEX WORDS: *Sandy tidal flats, morphodynamics, sediment budget, megatidal environment, tidal channels, LiDAR.*

INTRODUCTION

Tidal flats are highly dynamic environments subject to marine and terrestrial influences. Among these, sandy tidal flats (or sand flats) are complex environments controlled by a broad range of parameters such as strong wind-wave activity in what are usually low wave-energy environments, variability in tidal flows, and drainage. Although generally referred to as sand flats, these environments commonly exhibit high sediment heterogeneity reflected in a pseudo-cohesive and generally highly bioturbated mixture of sand, silt, and clay (Anthony, 2009; Yang *et al.*, 2007). Tidal flats are commonly present in tidal environments where sand supply is sufficient to infill a tidal basin or embayment. Feedback from morphological change, notably changes in the elevation of intertidal zones, affects the hydrodynamic regime and sediment transport (Moore *et al.*, 2009). Such interactions can lead to residual and spatial variations in sediment-flux convergence and divergence, resulting in net accretion and erosion, respectively. Inputs and/or internal redistribution of sediments within the tidal-flat system contribute to the sedimentation patterns and morphodynamic evolution of the salt marshes that are commonly associated with sand flats (*e.g.* Détriché *et al.*, 2011; Kolker *et al.*, 2009; Stevenson, Ward, and Kearney, 1988; Turner, Swenson, and Milan, 2000). Sand flats have been previously described from sites with very large tidal ranges such as the Bay of Fundy in Canada (Davidson-Arnott *et al.*, 2002), the Dee (Moore *et al.*, 2009) and other estuaries in the UK (Van der Wal, Pye, and Neal, 2002; Blott *et al.*, 2006; Mason, Scott, and Dance, 2010), and Mont-Saint-Michel Bay in France (Billeaud *et al.*, 2007; Bonnot-Courtois *et al.*, 2002; Desguée *et al.*, 2011; Larsonneur, 1994; Levoy *et al.*, 2017; Tessier, 1998; Tessier, Billeaud, and Lesueur, 2006).

The afore-mentioned studies show that the development of tidal flats is mostly governed by tidal currents. Waves can, nevertheless, play an important role (Anthony, 2009; Desguée *et al.*, 2011; Lee *et al*., 2004; Malvarez, Cooper, and Jackson, 2001; Reineck, 1967), especially at the lower seaward front of the flats where erosion commonly occurs. The higher landward part is usually dominated by tidal influence which commonly leads to

DOI: 10.2112/SI88-006.1 received 4 July 2018; accepted in revision 25 January 2019.
*Corresponding author: olivier.monfort@unicaen.fr
©Coastal Education and Research Foundation, Inc. 2019

accretion over time (Green and Coco, 2007; Janssen-Stelder, 2000; Kim, 2003). Under calm weather conditions, sediment transport is generally weak (Ralston and Stacey, 2007). Small waves can, however, enhance suspension of sediments which are subsequently transported by tidal currents (Anderson *et al.*, 1981). During storms, strong winds can generate energetic wind waves that are capable of mobilizing large amounts of sediment (Yang *et al.*, 2007).

Topographic/bathymetric surveys often constitute the main tool in unravelling the evolution of tidal basins over decadal/multi-decadal timescales. There is, however, a lack of studies on the morphodynamics of macrotidal/megatidal sand flats due to the limitations and inaccuracy of topographic techniques in the past, and difficulties inherent to measurements over very large surfaces. Anthony and Dobroniak (2000), Van der Wal, Pye, and Neal (2002) and Blott *et al.* (2006) used charts to quantify the magnitude of historical changes in tidal flats in estuaries. Some of these charts, commonly the more recent ones, are established from survey data obtained over a number of years, and, as such, do not represent the bathymetry at a single point in time.

LiDAR (LIght Detection And Ranging) has become established as a popular, though costly, remote-sensing system that collects spatially dense and accurate topographic data using airborne mounted lasers. It is one of the most suitable techniques for surveying large coastal areas (Brock and Purkis, 2009; Mason, Gurney, and Kennett, 2000; Pe'eri and Long, 2011; Saye *et al.*, 2005), but yet rarely used over vast tidal flats (Mason, Scott, and Dance, 2010.). Seasonal LiDAR surveys during low tide are particularly pertinent when studying the spatial and temporal variability of morphological changes over tidal flat environments. Airborne LiDAR acquisitions enable coverage of very large intertidal surfaces, often not easily accessible, and sometimes even hazardous, and a detailed description of morphologies due to a very high spatial resolution with densities exceeding 10 points/m² (Levoy *et al.*, 2016). Only airborne LiDAR technology offers the combination of large topographical coverage, almost instantly - at the same date - and a spatial resolution and precision useful for sand-flat studies.

Based on a LiDAR dataset comprised of 15 successive flights over the intertidal area of the Mont-Saint-Michel Bay (Normandy, France) between 2002 and 2017, we investigate, from event-scale to a decadal scale: (a) the spatial morphological variability of a sandy tidal flat and its tidal channel network in a megatidal setting associated with strong tidal currents and episodic storm conditions, (b) tidal-flat sediment budgets at these different timescales, and (c) the factors controlling the observed changes.

STUDY SITE

Mont-Saint-Michel Bay is located in the English Channel on the northwest coast of France, at the entrance of the Normandy-Brittany gulf between the Cotentin Peninsula and the Brittany coast (Figure 1a). The landward part is characterized by a shallow and large tidal sand flat comprising lower and mid-intertidal zones covering an area of about 210 km^2 backed by about 40 km^2 of upper-intertidal salt marshes dissected by tidal channels. The bay is world famous for its monastery (hereafter referred to as the monument) constructed in 1523 on a circular granite outcrop 82 m above MSL (the Mont), and which obtained the status of a UNESCO World Heritage site in 1979. The bay is also diverse in morphology and substrate sediment type as a result of variations in exposure to waves, tidal currents, winds, and tidal channel activity. The salt marshes front polders constructed over the last two centuries. The spatial distribution of the sediment cover over the intertidal area shows a decrease in grain size from the lower part of the tidal flat to the upper part (Figure 1b), reflecting the progressive reduction in energy affecting the bed (Larsonneur, 1989, 1994; L'Homer *et al.*, 1999). The lower and mid-intertidal zones mainly consist of fine sand and the upper intertidal zone of very fine bioclastic sand with 2-5% of clay (Desguée *et al.*, 2011), but areas closest to the salt marshes have an overall mud content (silt and clay) ranging from 20-25% that is locally named "tangue". According to the sand-silt-clay triangle of Van Ledden, Van Kesteren, and Winterwerp (2004), "tangue" is a non-cohesive sand-dominated sediment (textural bed type I). Macrozoobenthos is uncommon in this part of the intertidal area and is mainly composed of Corophium arenarium and Macoma balthica (Thorin *et al.*, 2001). The dominant salt marsh plant species are Spartina anglica and Puccinellia maritima which favour accretion and the trapping and storage of suspended sediments during high tides (Bonnot-Courtois and Levasseur, 2000; Détriché *et al.*, 2011; Neumeier and Amos, 2006). Three small rivers (Sée, Sélune and Couesnon, Figure 1a) with a mean water discharge of 8 to 15 $m^3.s^{-1}$ each, flow into the eastern part of the bay. However, the discharges are highly variable and can attain occasional values of up to 100 $m^3.s^{-1}$. The annual sediment supply of these rivers is considered as negligible (Larsonneur, 1994). The bay is reported to have been infilling rapidly in the course of the last 8000 years, with a mean accretion rate estimated at 2 cm per year (Larsonneur, 1994). This infill consists of sediments from the English Channel composed of about 50% bioclastic and 50% minerogenic sand and silt. The main identified sediment-transport pathway into the bay is located on the northern fringes and in the central part (Migniot, 1997). A secondary pathway occurs probably sporadically on the western side in front of the salt marshes near the monument (Gluard, 2012).

The regional setting is a megatidal environment characterized by the second highest tidal range in Europe with 8.5 m for mean tides and up to 15 m during very large spring tides (Levoy *et al.*, 2000). The bay is under the influence of the semi-diurnal tidal regime of the English Channel with a slight diurnal inequality. Currents during the flood are generally stronger than during the ebb, thus reflecting flood-dominated asymmetry for the tidal flats (Desguée *et al.*, 2011), and in much of the Couesnon channel (RIVAGES-GRESARC, 1998; Bonnot-Courtois *et al.*, 2002). This inequality is also marked by the ebb duration which is 1.17 times longer than that of the flood (Migniot, 1997). Tidal currents are strong, especially in tidal channels in the eastern part of the bay where ebb and flood currents attain up to 2 $m.s^{-1}$. Tidal bores are observed, especially during high spring tides in the Couesnon and Sée-Sélune channels with suspended sediment concentrations of up to 10 g/l (RIVAGES-GRESARC, 1996). Flood currents progress in the eastern part of the bay towards the southeast along the median axis of the bay and into the entrance of the estuarine area. Currents are weaker in the western part, ranging from 0.3 to 0.7 $m.s^{-1}$, but they are reinforced in the channels where mean velocities can exceed 2 $m.s^{-1}$ (Bonnot-Courtois *et al.*, 2002).

The modal winds are from W to NW, but during storms, strong S and SW winds can also occur, generating wind waves (Desguée *et al.*, 2011). Winds from SE and especially E are more episodic. Wave propagation is hindered by the shoreface bathymetry, by the Channel Islands, and by the presence of numerous shoals and archipelagos, all of which cause a decrease in wave heights over the shoreface (Levoy *et al.*, 2000). Consequently, locally generated low-energy waves prevail near the monument.

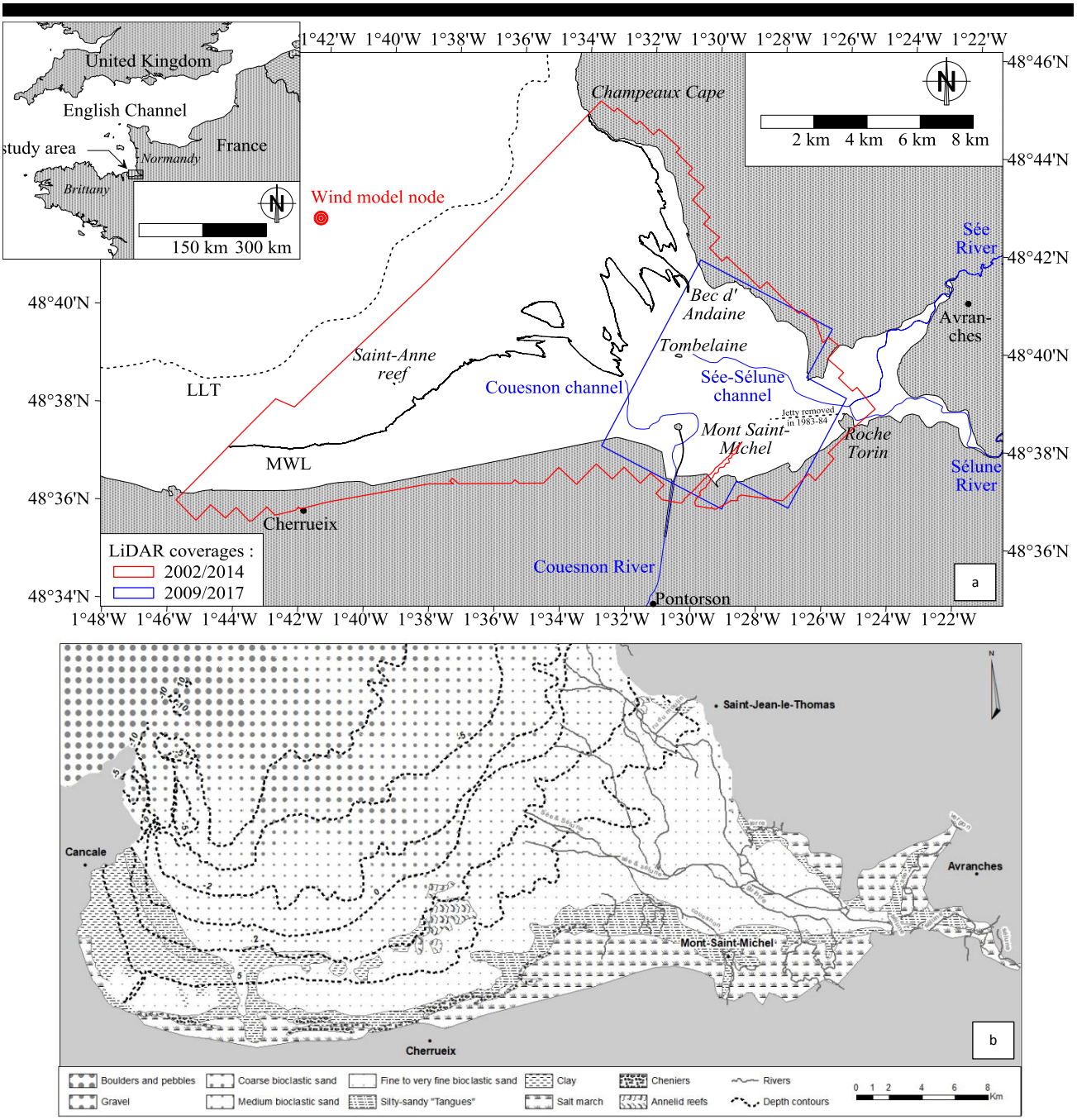

Figure 1. (a) Mont-Saint-Michel in Normandy, France, showing the study area and two sets of LiDAR coverages. These are referred to in the text respectively as '2002/2014' and '2009/2017'. The former refers to two surveys in 2002 and 2014 covering a large area of the bay at spring low tide, whereas the latter consists of 14 surveys over a smaller area of the bay; (b) spatial distribution of sediment grain sizes and bathymetric contours (after Tessier, Billeaud, and Lesueur (2006), and Weill *et al.* (2012)).

However, Desguée *et al.* (2011) showed that waves can enhance suspension and thus active sediment transport. They proposed that the upper tidal flat close to the salt marshes can be considered as a mixed wave-tide-dominated coastal environment in the sense of Anthony and Orford (2002), controlled mainly by tidal currents, but also strongly affected by waves.

METHODOLOGY

Two sets of LiDAR data were collected between 2002 and 2017 (Table 1). The first set was acquired in September, 2002, by the Institut français de recherche pour l'exploitation de la mer (Ifremer), and was provided directly in Digital Elevation Model (DEM) format with a mesh size of 2 m. The second dataset consisted of 14 seasonal surveys conducted within the CLAREC project (acronym for Contrôle par Laser Aéroporté des Risques Environementaux Côtiers) between February 2009 and May 2017 using a Leica ASL60 (see Levoy *et al.*, 2013, for this system's technical details). The CLAREC project provided DEMs with 1 m-grid size. The x and y coordinates are relative to the Lambert 93 French National Grid, and the height, z, refers to the IGN reference level (French Ordnance Datum), which is close to the mean sea level.

The coverage areas of these datasets are shown in Figure 1a and Table 1. The '2002/2014' coverage refers to surveys in 2002 and 2014 that cover much of the intertidal area, enabling calculation of sediment budgets of the bay above the lowest low-tide level. The '2009/2017' surveys conducted over a smaller area of the bay covered the upper part of the intertidal system (about 52 km²), just above the mean water contour (Figure 1a).

The vertical root mean square error (RMS error) can be estimated by taking into account several topographic profiles of the road leading to the Mont-Saint-Michel monument.

Table 1. *LiDAR datasets: dates of surveys, sources and coverages.*

Dates of the aerial LiDAR surveys	Sources	Coverage (fig.1a)
September, 2002	Ifremer	Large area
February 12, 2009	CLAREC project	Small area
September 21, 2009	CLAREC project	Small area
April 18, 2010	CLAREC project	Small area
September 22, 2010	CLAREC project	Small area
April 18, 2011	CLAREC project	Small area
August 31, 2011	CLAREC project	Small area
May 12, 2012	CLAREC project	Small area
October 15, 2012	CLAREC project	Small area
May 26, 2013	CLAREC project	Small area
May 15, 2014	CLAREC project	Large area
June 3, 2015	CLAREC project	Small area
March 13, 2016	CLAREC project	Small area
October 3, 2016	CLAREC project	Small area
May 9, 2017	CLAREC project	Small area

Using 1276 points on each profile, the calculated RMS error was less than 0.10 m, which is good and close to RMS values frequently cited in the literature (*e.g.*, Levoy *et al.*, 2016; Liu, 2009; Sallenger *et al.*, 2003; Zhang *et al.*, 2005).

As reported in recent studies, considerations of uncertainty in DEM surface representation are crucial in the ability to identify and compare important changes in dynamic environments (Eamer and Walker, 2013; Lane, Westaway, and Hicks, 2003; Wheaton *et al.*, 2010). DEM error depends on survey-point quality, sampling strategy, surface composition, topographic complexities and interpolation methods (Heritage *et al.*, 2009). A commonly adopted procedure for managing DEM uncertainties involves specifying a minimum level of detection threshold (minLoD) to distinguish actual surface changes from inherent noise (Fuller *et al.*, 2003). Previous studies (Brasington, Langham, and Rumsby, 2003, Wheaton *et al.*, 2010) have reported that individual errors in the DEM can be propagated into the DoD as:

$$\delta u_{DoD} = \sqrt{(\delta z_{new})^2 + (\delta z_{old})^2} \qquad (1)$$

where δu_{DoD} is the propagated error in the DoD, and δz_{new} and δz_{old} are the individual errors in DEM_{new} and DEM_{old}, respectively. The assumption of this method is that errors in each cell are random and independent.

In this study, the minLoD was based on the uncertainty threshold of the DEMs and its propagation into the generated DoD. Hence, the uncertainty threshold of the DEMs is 0.1 m, which leads to a propagating uncertainty of 0.15 m (DoD). This latter value was used to remove point cells where elevation change values did not attain the precision of the computation procedure, thus making it possible to identify areas of significant morphological changes.

As indicated by Chassereau, Bell, and Torres (2011), LiDAR data provide a rather poor description of the microtopography of salt marshes, and can introduce a positive spatially variable bias of about 0.10-0.15 m (Gopfert and Heipke, 2006) due to limited LiDAR penetration through most marsh vegetation (Schmid, Hadley, and Wijekoon, 2011). In order to avoid significant errors and to obtain realistic quantitative results on sediment budgets at seasonal to decadal timescales, the salt marshes are not included in the calculations.

The LiDAR system used is also limited in its penetration of water within the tidal channels but it can record reflectance intensity of the surface. Intensity provides useful information for detecting wet channels because of the strong absorption of light energy by water and the high spatial resolution of intensity data (Chust *et al.*, 2008; Hooshyar *et al.*, 2015). For each survey, an image of intensity values of the study area was used to locate the main channels. As for salt marshes, the tidal channels were not integrated in the calculation of the sediment budget. The channels are a potential storage zone, covering 8.5% of the '2002/2014' area (Figure 1a), i.e., about 3.7 Mm². The channels can potentially store or release about 1 Mm^3 of sediments with an accretion or erosion of only 0.3 m. As a result, it is currently not possible to calculate with certainty and a good degree of accuracy the complete sediment budget of tidal flats. Even using LiDAR technology, the approach adopted here regarding estimation of the sediment budget remains qualitative without considering salt marshes and channel areas but with an applied minLoD of 0.15 m.

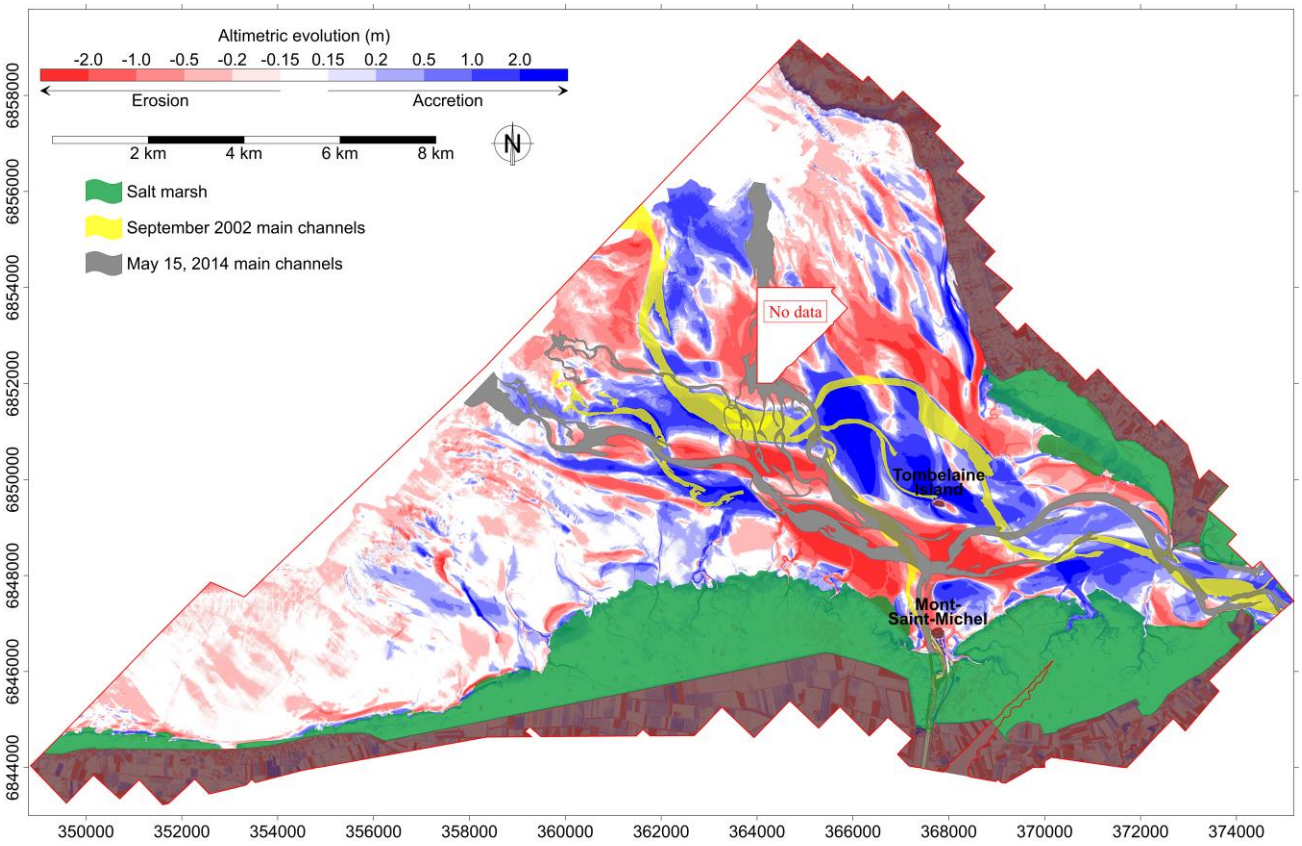

Figure 2. Topographic changes in the bay between 2002 and 2014. The salt marshes (green surfaces) and the main tidal channels (yellow and grey surfaces) are intertidal areas excluded from sediment budget calculations. Continental surfaces are in brown.

RESULTS

Morphological Changes and Sediment Budgets

Decadal Timescale

The DoD 2014-2002 (Figure 2) highlights the changes that have affected the intertidal zone of much of the bay with a relatively high spatial resolution and an accurate elevation change estimation. Erosion or accretion can attain up to 2 m, but locally values larger than 2.5 m are observed, especially seaward of the area between the monument and Tombelaine island (Figure 1).

The main changes are associated with channel migrations along the main axis of the system oriented NW-SE, and these changes have affected both the upper and lower parts of the estuarine system.

Even though the quality of data from the LiDAR device is good (rms error < 0.1 m), volume calculations over large surfaces must be considered as orders of magnitude. All surfaces where elevation variations were between -0.15 m and +0.15 m were excluded from the calculation. As these variations are more or less randomly distributed, their contribution is considered not significant. Table 2 shows the results of the sediment budget calculation. Over the 2002/2014 coverage area (Figure 1a), the eroded surfaces in the 12 years that elapsed between these two dates (46 Mm^2) were greater than those where residual accretion occurred (35.8 Mm^2). In contrast, the mean accretion was about 0.8 m while the mean erosion was -0.7 m. The volume of accretion was close to 30 Mm^3 whereas the volume of eroded sediments was about 34.4 Mm^3. The volumetric margins of error were comprised between 3.6 and 4.6 Mm^3, indicating that the measured volumetric changes were significant. With these results, the sediment budget of the tidal flat could have been negative, to the tune of around -4 Mm^3, over the 12-year period.

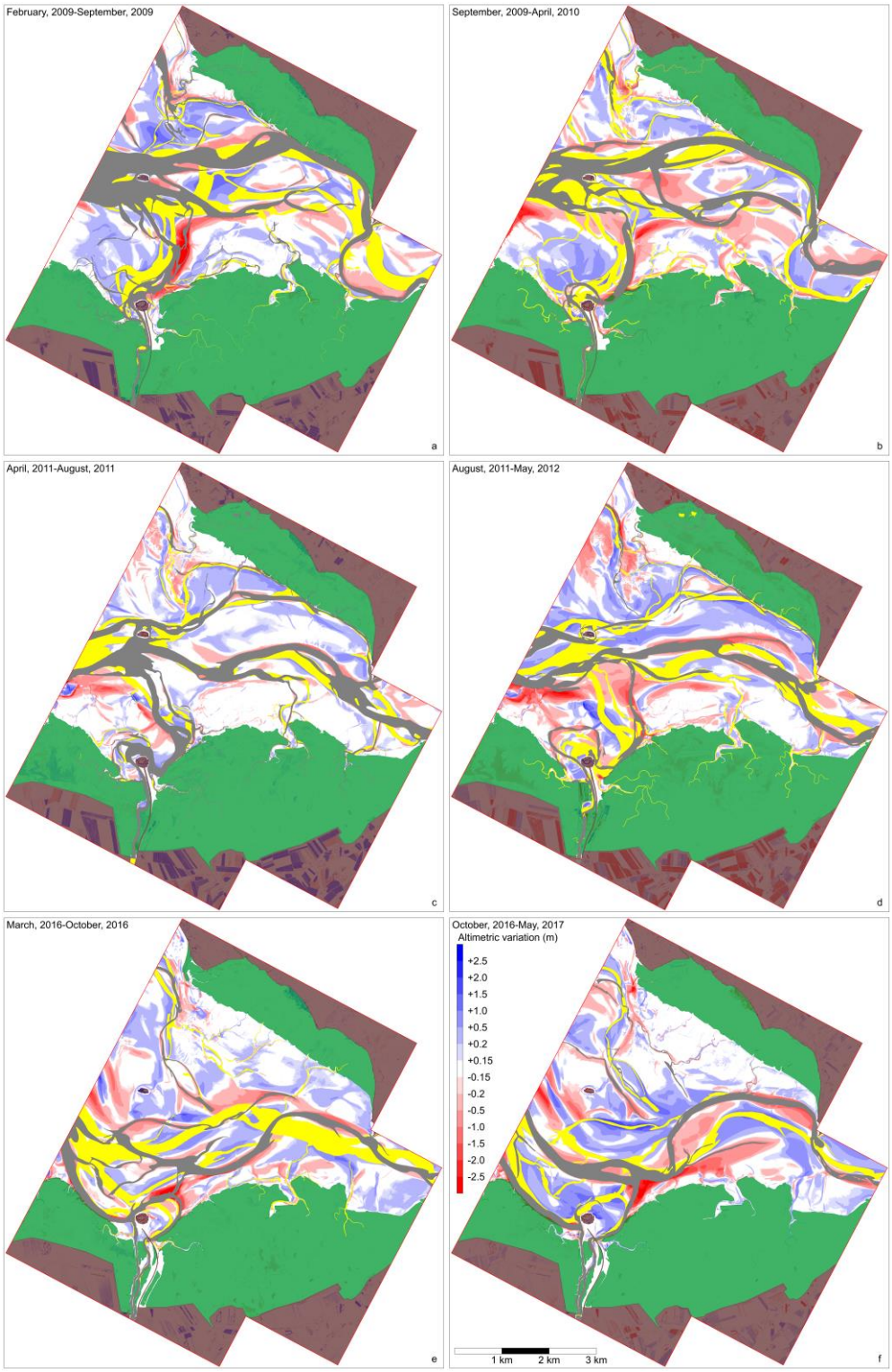

Figure 3. Seasonal topographic changes from 2009 to 2017 and positions of the Sée-Sélune and Couesnon channels. The salt marshes (green surfaces) and the main tidal channels (yellow and grey surfaces) are intertidal areas excluded from sediment budget calculations. Continental surfaces are in brown.

Table 2. *Accretion and erosion, error margins, and sediment budget of the intertidal zone up to the level of the marsh area between 2002 and 2014.*

2002 - 2014 changes (> | 0.15 m |)	Accretion	Erosion
Mean of elevation change (m)	0.8	0.7
Surface (Mm^2)	35.8	46.0
Volume (Mm^3) with margins of error	30.2 ±3.6	34.4 ±4.6

Annual and Seasonal Timescales

The erosion and accretion areas identified from the 14 LiDAR surveys of 2009-2017 (Figure 3) are mainly elongated and sinuous, clearly pointing to a link between the topographic changes and the positions and lateral migration of the main channels over time.

Accretion occurred between May 2012 and May 2014 in areas where the Couesnon was initially located, and erosion prevailed over the northern part of the tidal flat in front of the monument (Figure 3). The other main topographic changes were due to the migration of the Sée-Sélune from a northerly location in 2009 to a central position in 2013 close to the median axis of the bay. The changes induced by the lateral migration of these channels contributed to a tidal-flat bottom elevation growth of up to 1.5 m. The 2009-2017 LiDAR surveys were used to identify topographic changes at seasonal and annual timescales (Table 3). They highlight the variability of sediment budgets, especially at a seasonal timescale, with a positive budget > 1.1 Mm^3 (May to October 2012) and a negative budget > 0.3 Mm^3 (September 2009 to April 2010). At an annual timescale, the same remark is also true, even though between February 2009 and May 2012, a noteworthy stability, with a value of about +0.4 Mm^3/y, prevailed. Indeed, significant erosion of the order of -1.6 Mm^3 occurred between May 2013 and May 2014, whereas about +0.9 Mm^3 of sediments accumulated in the bay the year before.

Basin Hypsometry

In order to obtain an integrative view of the intertidal evolution that includes the salt marshes, two hypsometric curves have been computed respectively for the 2002 and 2014 DEMs. These curves represent the total wetted surface area of a tidal flat system as a function of elevation, and provide a better representation of the actual shape of the substrate (Kirby, 2000) than classical single cross-shore profiles that can also be used to define the topographic shape over an entire tidal flat. Such curves allow an irregular basin topography to be smoothed by longshore integration (Friedrichs, 2011). The shape derived from the hypsometric curves does not exhibit pronounced concave-up or convex-up shapes that are generally associated, respectively, with wave dominance (Zimmermann, 1973) and tide dominance (Friedrichs and Aubrey, 1996), but rather shows a relatively regular slope (Figure 4).

However, the shape becomes concave-up around the mean high water spring (MHWS) level. Accretion is observed slightly around the mean water level but especially just under MHWS level whereas erosion is characteristic of the rest of the curve except for slight accretion between +1 and +2.5 m IGN69 (French datum), just above the mean sea level (MSL). This curve does not reach the lowest level of the sea (-6.7 m IGN 69), but the lowest parts of the bay show deposition between 2002 and 2014. Various authors have noted that erosional flats, especially mudflats, tend to be low and concave-up (Bearman *et al.*, 2010; Gratiot, Gardel, and Anthony, 2007; Kirby, 2000; Mehta, 2002). In these studies, erosion is also associated with offshore transport, wave dominance and coarser sediments (including mud pebbles eroded from consolidated muddy substrates). Using the same hypsometric approach, over the 2009/2017 coverage, Figure 5 confirms the erosion of much of the intertidal zone above MSL between 1.5 and 5 m and large regular accretion on the upper part around MHWS.

Table 3. *Seasonal and annual sediment budgets between 2009 and 2017. Dz is the mean positive or negative elevation change in the study area (sediment budget divided by the surface area). Dz-pos is the mean elevation change of the accretion surfaces. Dz-neg is the mean elevation change of the erosion surfaces.*

Dates of surveys	Seasonal budgets (m^3)	Dz (m)	Dz-pos (m)	Dz-neg (m)	Annual budgets (m^3)
Feb - Sept 2009	741 226	0.08	0.43	-0.58	Feb 2009 - Apr 2010
Sept 2009 - Apr 2010	-373 319	-0.03	0.37	-0.51	367 907
Apr - Sept 2010	-51 341	0.00	0.35	-0.50	Apr 2010 - Apr 2011
Sept 2010 - Apr 2011	459 576	0.04	0.44	-0.60	408 235
Apr - Aug 2011	456 644	0.05	0.34	-0.44	Apr 11 - May 12
Aug 2011 - May 2012	-48 160	0.00	0.44	-0.60	408 484
May - Oct 2012	1 126 568	0.10	0.42	-0.73	May 2012 - May 2013
Oct 2012 - May 2013	-204 262	-0.02	0.47	-0.67	922 306
May 2013 - May 2014		-0.11	0.49	-0.84	-1 663 836
May 2014 - June 2015		0.05	0.53	-0.69	700 585
June 2015 - March 2016		0.03	0.52	-0.79	440 764
March 2016 - Oct 2016	355 475	0.03	0.35	-0.52	March 16 - May 17
Oct 2016 - May 2017	1 069 648	0.08	0.48	-0.62	1 425 123

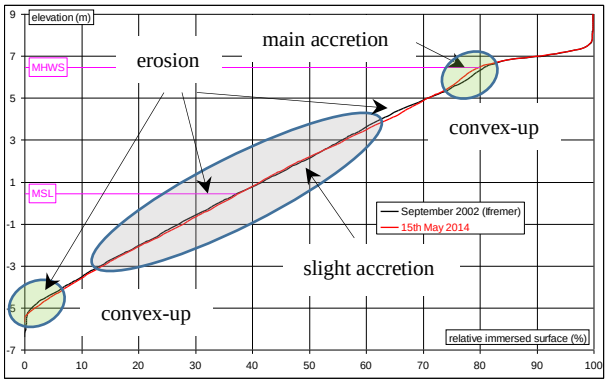

Figure 4. Hypsometric curves of the larger bay area associated with the 2002/2014 coverage. MSL = Mean sea level; MHWS = Mean high water spring tide level.

The negative sediment budget (-4.2 Mm^3, Table 2) between 2002 and 2014 in the larger study area contrasts with the dominance of accretion above MSL in the smaller study area between 2009 and 2017 (+3 Mm^3, Table 3). Clearly, this would appear to confirm that at a timescale of several years accretion dominates on the upper part of the system, especially above MSL over the '2009/2017' coverage area, and erosion on the lower intertidal zone covered by the 2002/2014 surveys, as reflected by the hypsometric curves (Figures 4 and 5).

These contrasting patterns reflect a diminishing wave-energy gradient towards the low-energy salt marshes resulting from the combination of flood-dominant tidal current asymmetry and the dominance of onshore sediment movement during stormy conditions (Desguée *et al.*, 2011) on the upper part of the system, balanced by erosion in the middle and lower parts of the sand flats.

Tidal Channel Migration

The time series of the locations of the Couesnon and Sée-Sélune tidal channels reveal an interesting behaviour that contributes to explaining the morphodynamics of the tidal flat system. The Couesnon channel migrated gradually from W to E in the course of the first ten years (2002-2012), forming a very large meander around the monument in May 2012 (Figure 6). The eastward migration of the Couesnon close to the monument resulted in continuous erosion of the upper tidal flat between February 2009 and May 2012. The pictures taken on 12 May 2012 (Figure 7) show the meander loop of the Couesnon around the monument but also a very shallow northward-oriented channel linking the meander to the Sée-Sélune channel located in a very southerly position. The following LiDAR topography on May 2013 shows an important modification of the location of the Couesnon channel, directed northward close to the monument, and afterwards northwestward, with an axis parallel to that of the Sée-Sélune. Up to June 2015, the confluence between the two channels moved from W to E and from E to W, but, overall, the Couesnon remained oriented northward, without a large meander.

The location of the joint Sée-Sélune channel also changed but in several steps. Between 2002, when only one channel was visible, and April 2010, the channel moved northward, but a small secondary channel observable in 2009 and April 2010 (Figure 3) was present in the median axis of the system. Between April and September 2010, the north Sée-Sélune channel and the central one had approximatively the same width, but between September 2010 and May 2012, the median channel became more dominant, whereas the northern one became progressively abandoned. Finally, a back-and-forth movement was observed for the Sée-Sélune, while the Couesnon moved eastward. After May 2012, the Sée-Sélune was located in the central axis of the bay, but south of Tombelaine island, close to the Couesnon (Figure 3).

Between February 2009 and May 2012, the eastward migration of the Couesnon and the formation of a large meander progressively occurred. These are probably due to the interaction of sediment input from W northwestward of the monument and meander-bend scouring and enlargement by the ebb current. In contrast, the changes between May 2012 and May 2013 occurred at a different timescale. No topographic data are available between these two dates, but a WorldView-1 satellite image on 25 May 2012, taken only a couple of weeks after the LiDAR flight, shows clearly that the Couesnon was already located northward at this date, and with a NW orientation, proving the event timescale of this morphological change (Figure 8).

The antecedent morphology of this sudden change can be analyzed from the 12 May 2012 LiDAR data and associated aerial picture (Figure 7). A small channel was already present between the Couesnon and the Sée-Sélune, but the relief in the picture shows clearly a morphology of sand-bank incision and head erosion, observed just after spring tides with strong currents, and enhanced by the reduction of the distance and consequent slope-steepening between the two channels over a one-year period (Figure 9). These changes were thus favorable to the channel capture observed a few days later on the WorldView-1 May 25 2012 satellite image (Figure 8). Eye-witness accounts indicate that the Couesnon suddenly abandoned the large meander to flow straight ahead and join the Sée-Sélune overnight between May 22 and 23, 2012. It should be noted that this happened before the low-water releases scheduled from the Couesnon dam became fully operational.

The time series of LiDAR images provide an illustration of the highly dynamic channel migration processes in the tidal flat area of Mont-Saint-Michel Bay. The most remarkable aspects observed are:

(1) The rapid development of large channel meanders. Channel migration rates are more than a factor 10 larger than those reported for the Venice Lagoon and other estuaries (Finotello *et al.*, 2018). High mobility of tidal flat sediments (small grain size, low cohesion) is probably an important factor.

(2) Very sudden meander avulsion by chute-channel formation.

The LiDAR images suggest that such events involve complex interactions within the channel network.

Both features are probably also due to the very high tidal range in the bay, which produces strong tidal currents in the channels as well as over the tidal flats.

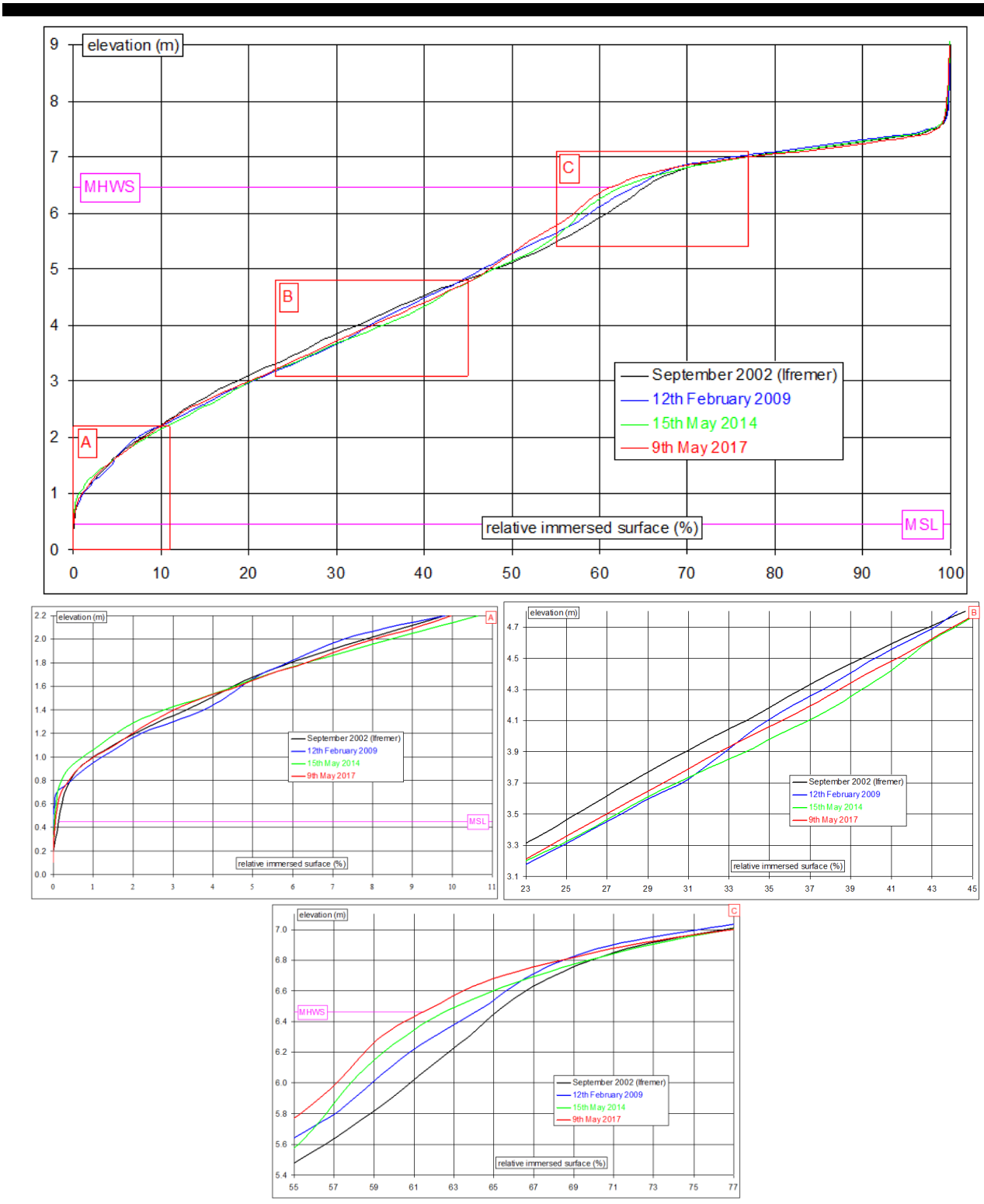

Figure 5. Hypsometric curve of the 2009/2017 coverage (see Figure 1a) between 2002 and 2017 and close-up views (A, B, C) of representative portions of the curve.

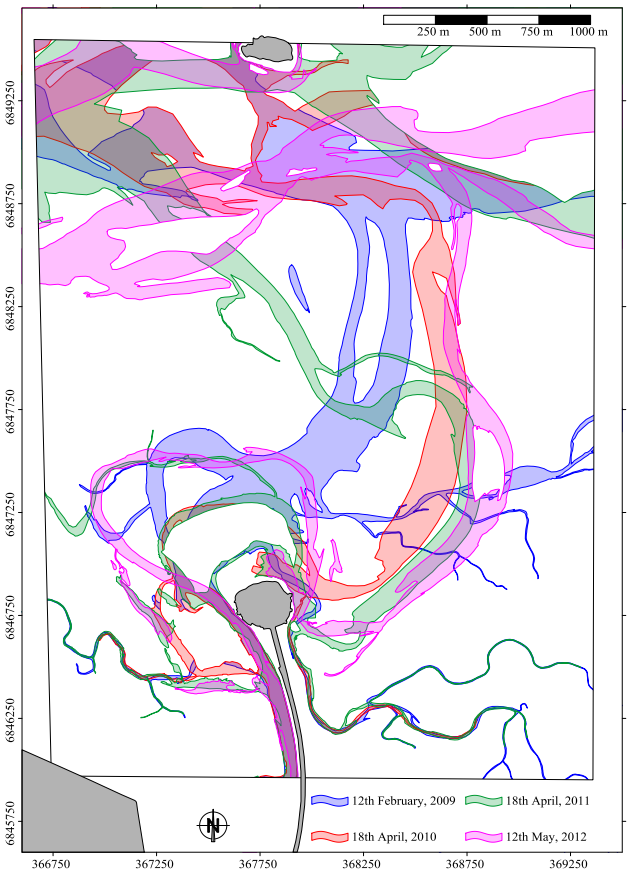

Figure 6. Eastward migration of the Couesnon meander located close to the monument from 2009 to 2012.

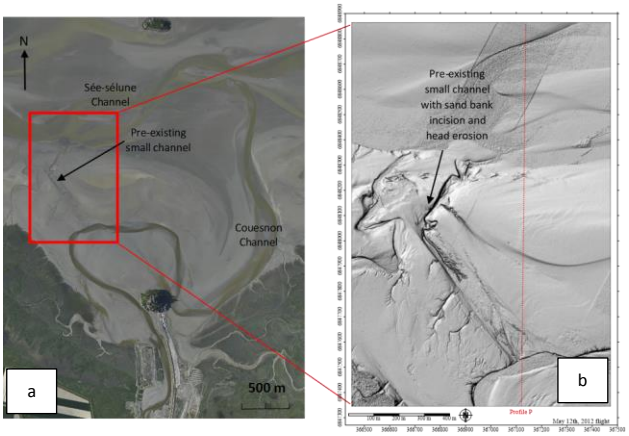

Figure 7. Aerial photograph of the Couesnon meander and Sée-Sélune channel on 12 May 2012 (a) and detailed view of the topography between these channels showing a deep incision of the sand bank by the former channel prior to its capture by the latter (b).

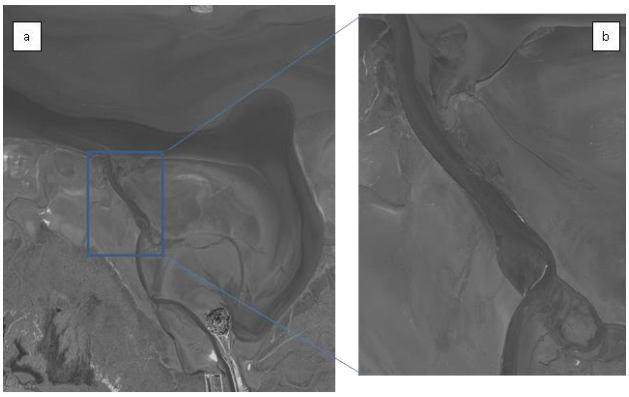

Figure 8. WorldView-1 satellite image (a) and zoom (b) on 25 May 2012 attesting to a sudden change in the location of the Couesnon.

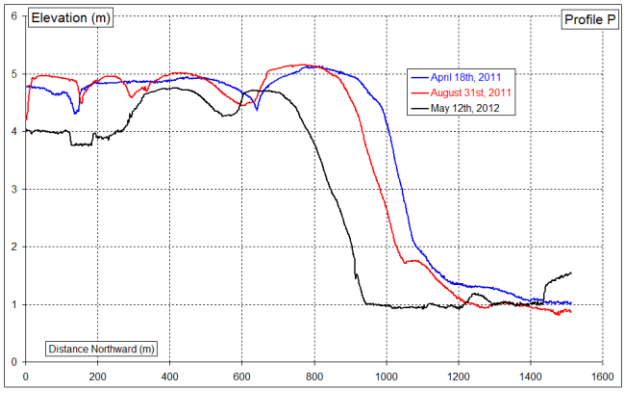

Figure 9. N-S profiles linking the Sée-Sélune and Couesnon channels between April 2011 and May 2012, and showing the rapid southward migration of the former (profile location in Figure 7b).

DISCUSSION

Decadal-scale Morphological Change and Sediment Budget

The LiDAR datasets are too short for studying long-term morphological change. An analysis of long-term morphological behaviour by Levoy *et al.* (2017) highlighted the important role of the 18.6-year lunar nodal cycle. Due to the influence of long-term forcing mechanisms, it is useful to replace the two study periods of LiDAR surveys in a longer timescale to understand the main morphological changes at a shorter time scale. The morphological changes of the 2002-2014 study period (large LiDAR area, Figure 1) covered, between 1997 and 2007, a decreasing M2 tidal range, and between 2007 and 2015 an increasing M2 tidal range. The 2009-2017 study period (small LiDAR area, Figure 1), in relation with seasonal morphological changes, covers mainly the last complete limb of increasing M2 tidal range and the beginning of the last decreasing tide-range limb. Levoy *et al.* (2017) present evidence for a relationship between the changing tide range from low to high phases of the nodal cycle and morphological changes of tidal flats of the Mont-Saint-Michel Bay. The primary mechanism, which links nodal tidal range and topographical evolutions, is changes in tidal prism

and current velocities in this shallow large tide-range bay that are matched by increasing or decreasing flood-dominated asymmetry during the 18.6-year nodal tidal cycle. The location of the Sée-Sélune channel can be considered as a proxy in response to the reinforced/diminished flood-dominated asymmetry during increasing/decreasing M2 tidal ranges, which generates sediment import/export. The channel was located along the southern flanks in 1996-2000 and 2012-2015 and along the northern flanks of the bay in 2007-2010. The Sée-Sélune channel moved northward from the central axis of the bay and then swung back southward in a typical seesaw movement. Over the same time, the Couesnon also migrated over a large swathe, moving from west to east, and suddenly back to west. The consequences of these channel migrations from a morphological point of view are, between 1997 and 2007 (decreasing M2 tidal range), the main erosion areas located in the northern part of the bay, in front of a well-developed salt marsh and around Tombelaine island. Accretion is mainly observed in the centre of the bay. Between 2007 and 2015 (increasing M2 tidal range), a dominant erosion zone is found in the southern part of the bay in front of the salt marshes west and east of the monastery. Accretion occurred in front of the northern salt marshes, around Tombelaine island, exactly where erosion was observed in the course of the previous period. In addition, between 1997 and 2007, the sediment budget is slightly positive with a gain of only 18 800 m^3 over the intertidal area, whereas a net accretion of 1 Mm^3 is observed for the phase of increasing M2 tidal range.

Between 2002 and 2010, the Sée-Sélune was influenced by a phase of the lunar nodal cycle with relatively low tidal ranges. During this period, flood-dominated asymmetry diminished and weaker tidal currents resulted in a more balanced bay sediment budget. However, the channel moved southward, between 2010 and 2014, in relation with the nodal limb of increasing tidal amplitudes that induced reinforced sediment import and preferential accretion of the intertidal flats. The sediment budget, excluding channels and the marsh area, is negative (4 Mm^3) over the period 2002-2014 and the hypsometric curves indicate accretion close to MHWS and mainly erosion below this level. These trends suggest a complex pattern of sediment transfer from the lower towards the upper part of the flats, but perhaps also offshore, outside of the study area, and eventually, from the intertidal zone towards the channels, for which, unfortunately, no topographic data are available.

Sediment input from the outer subtidal bay is low because pebbles and gravels are located just under the lowest water level (Larsonneur, 1994, Tessier, Billeaud, and Lesueur, 2006; Weill *et al.*, 2012; Figure 1b). The source of sandy materials is very limited near the borders of the intertidal bay and significant sand inputs are only possible in the northern part of the bay under the action of NW waves from the west coast of the Cotentin Peninsula. Only bioclastic production can lead to input of a significant volume of sediments, but the renewal timescale of this type of sediment is unknown.

Relationship between Seasonal Sediment Budgets and Wind

The response of the large-scale morphology of tidal flats to change induced by waves or tidal currents is relatively slow, when compared, for instance, with beach environments. One of the reasons pointed out by Pethick (1996) and Friedrichs (2011) is that tidal flats are generally very low-energy systems with large flat areas over which wave attenuation can be very important. However, other authors have monitored a seasonal behaviour pattern in tidal flats, with, classically, deposition in summer and erosion in winter (Kirby and Kirby, 2008; Ryu *et al.*, 2008), or tidal flat slopes increasing in summer and decreasing in winter (Pethick, 1996). This observation regarding seasonal behaviour is partly borne out by the present dataset. A relationship between tidal flat elevation and wind speed, taken as a surrogate for wave height, is often proposed to explain this behaviour (Kirby and Kirby, 2008; Yang, Ding, and Chen, 2001). Christiansen *et al.* (2006) indicated that, in addition to wind-induced wave activity, winds may also influence current directions, especially at low water depths. As shown by Héquette, Hemdane, and Anthony (2008), strong winds blowing in the same direction as tidal flow can significantly reinforce tidal currents, even if the direction of the net sediment transport is largely determined by the asymmetry of tidal flows in shallow waters. Conversely, strong winds can limit tidal current speeds when blowing in the opposite direction. Consequently, sediment fluxes and direction strongly depend on wind velocity and direction with changes in flux orientation from the ebb to the flood.

In Mont-Saint-Michel Bay, the sensitivity of the sediment budget to wind and wave conditions seems high. Large positive budgets are observed in summer (data for February and September 2009, April and August 2011, May and October 2012, and March and October 2016) and large negative budgets in winter (data for September 2009 and April 2010, and October 2012 and May 2013). Only the 2010-2011 and 2016-2017 winters show a large positive budget.

Measured local wind data are not available for the study period. A numerical model developed by the French meteorological office has thus been used to calculate the wind characteristics at a central location of the bay (1°42’ W, 48°42’ N, Figure 1a). For each period between two consecutive LiDAR flights, tri-hourly wind speed and direction have been extracted and visualized using a wind-rose graph (Figure 10). From a qualitative point of view, wind direction, especially for strong winds (> 8 m/s), seems to influence the sediment budget. Figure 10 shows that the dominant strong NW winds (black circles), mainly in summer, associated with complementary SW winds (red circles), between two LiDAR flights, contribute to a positive sediment budget, especially when E winds are rare and weak as during the fair-weather period between May and October 2012 (+1.1 Mm^3). Winds from S (blue circles) and NE (green circles), mainly in winter, could contribute to reducing significantly sedimentation over the intertidal sand flats. The NW sector (from WNW to NNW) seems to induce sediment import into the intertidal zone. In contrast, a negative sediment budget is observed when strong winds from SW to SE are dominant as during the winter period between September 2009 and April 2010. Rather long-fetch waves associated with NW winds favour sediment supply to the upper part of the system, *e.g.* the smaller '2009/2017’ study area located above MSL. Winds blowing from land (from S to NE) do not notably influence wave heights within the bay, but probably modify tidal currents especially when water depths are low, and probably contribute to sediment export offshore, as also observed by Christiansen *et al.* (2006) in the Danish Wadden Sea. This

occurs as winds counter flood currents while reinforcing ebb currents. SW winds always observed during summer periods seem favorable, probably at a lower level, to the import of sediment towards the bay, just like NW winds. These SW winds generate short waves that arrive from a W direction following refraction within the bay at high tide. The sediment budgets are very low (close to -50 000 m^3) for two periods: April 2010-September 2010, and August 2011-May 2012. The two wind roses exhibit peculiarities in comparison with those previously mentioned. Between April 2010 and September 2010, the NW sector was dominant but the SW and NE sectors were also clearly important. As mentioned previously regarding the influence of wind direction on sediment movements in the bay, inputs favoured by winds from the NW, and secondarily from SW, seem to be counterbalanced by outputs induced by strong NE winds. The same interpretation goes for the period between August 2011 and May 2012. Even though the wind directions are better balanced, winds from NW seem to be countered by those from SW to SE. In winter, clearly strong winds from S contribute to sediment export from the intertidal area. Note that the negative annual sediment budget (-1.6 Mm^3) between May 2013 and May 2014 was observed during a period of exceptional duration of strong winter winds from S. Masselink *et al.* (2016) demonstrated that this was the most energetic winter along much of the Atlantic coast of Europe since at least 1948.

For the October 2016 to May 2017 period (+1 Mm^3), NW and SW wind sectors are significant, as during summer, and can explain the positive sediment budget even though SE winds were dominant and contributed probably to export of sediment from the study area.

Although Figure 10 suggests a relationship between wind characteristics and the sediment budgets between surveys, the positive sediment budget between September 2010 and April 2011 is rather peculiar. Two wind sectors were dominant, NE and SW, which, as said previously, preferentially contribute to a well-balanced sediment budget, with probably weak sediment import associated with SW winds being countered by export due to NE winds. However, the sediment budget was significantly positive at +459 000 m^3. A substantial duration of strong NW winds was observed, but this clearly cannot explain the positive budget.

Relationship between Seasonal Sediment Budgets, River Discharge and Specific Features of Mont-Saint-Michel Bay

The foregoing suggests that other factors, in addition to wind, waves and tides, influence the sediment budget of the intertidal sand flats of Mont-Saint-Michel Bay. The shallowness of tidal channels (low-water depth of the order of 1 m and up to 200 m wide), in spite of strong tidal currents with an erodible substrate, is indicative of a high sediment mobility that precludes the development of steep channel slopes. In addition, large water depths over the tidal flats (several metres at spring tides), favourable to strong currents and high mass transport over these

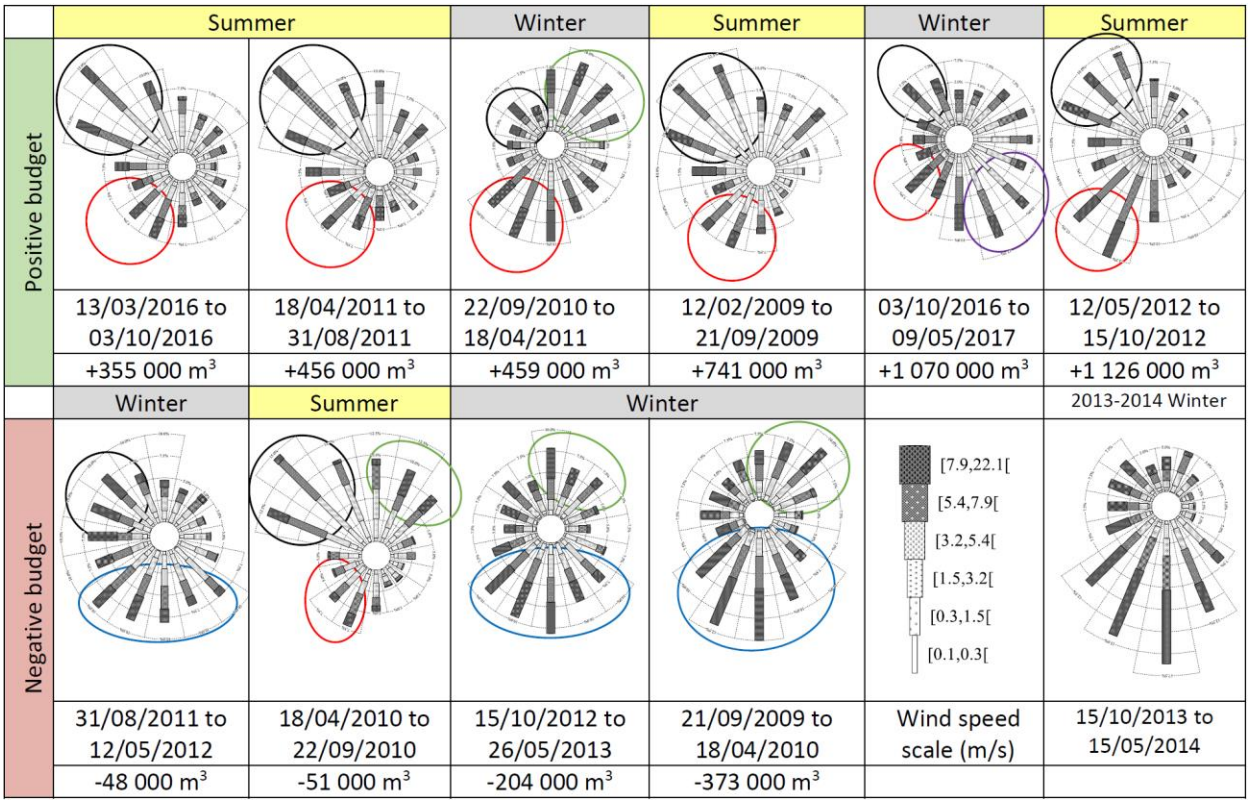

Figure 10. Seasonal wind roses and associated bay sediment budgets between February 2009 and May 2017.

flats, imply that sediment accommodation space is still high over these flats. The channel configuration in the bay can change extremely rapidly: local channel shifts by more than 10 metres in a single tide and more than 100 metres in a full neap-spring tide cycle have been observed in the field; meander avulsion in favour of a chute channel occurs within a few tidal cycles. Notwithstanding, there is no reason to believe that the morphodynamic processes in the bay are fundamentally different from other tidal bays in the world, but due to the above-mentioned features these processes probably show greater amplitude and act at shorter timescales.

In this specific context of sediment features and tidal range, one other obvious influence is related to multi-annual fluctuations in river runoff. The daily water discharges of the Couesnon are shown in Figure 11. The discharges of the Sée and Sélune exhibit a similar pattern. Winter runoff is higher than summer runoff, but not always to the same degree. The winters of 2010-2011, and 2016-2017 were extremely dry, whereas the winters of 2012-2013 and 2013-2014 were exceptionally wet. River runoff during these wet winters could have reinforced ebb currents sufficiently to evacuate sediment from the inner bay to the outer bay, thus contributing to the negative sediment balance for the May 2013-May 2014 period (Table 3). During very dry winters, river runoff cannot counter the general landward sediment transport by tides and winds. This is deemed to have been the cause of the high net sedimentation for the periods April 2010-April 2011 and March 2016-May 2017 (Table 3).

Anthropogenic versus Natural Influences

As in many European estuaries and embayments, large areas of land were reclaimed in the nineteenth and twentieth centuries in Mont-Saint-Michel Bay, generating accelerated deposition (Pethick, 1996). Polders are mainly located in the southern part of the bay, close to the monument (Figure 1a). The Roche Torin dike was built in 1860 to prevent the southward migration of the Sée and the Sélune and to ensure the security of some of the land reclamations (Figure 1a). A road providing easy access to the monument was built in 1879. This road acted as a barrier to tidal flow and generated increased sedimentation in the southern part of the bay. A dam was also built in 1969 on the Couesnon to block the tidal intrusion and associated flooding. Gates were closed during the flood and opened during the ebb for the discharge of fluvial water (Larsonneur, 1994). The combined effect of all of these works has been to limit the erosional effects of channel meandering and to reduce the tidal prism, resulting in enhanced sedimentation in certain areas. In the 1970s, a project to restore the maritime character of Mont-Saint-Michel Monastery began. The project was designed to prevent accretion and the encroachment of salt marshes on the monastery by restoring a large area of sandy tidal flats close to the rock outcrop on which stands the monument. A new dam was built in 2009 to harness the hydraulic capacity of the Couesnon river by storing and releasing fluvial and tidal waters over a short period around low tide, in order to erode sediment close to the Mont. The maximum water discharges are up to 100 m^3/s, but they depend on the tidal range and the river discharge. The old road allowing vehicle access to the monument was removed in 2015 and a new bridge enabling tidal through-flow was built to restore tidal current action close to the monument. Other complementary works upstream and downstream of the dam were implemented to increase the water volume releases by the dam and to improve the competence of this flux in removing sediment close to the Mont.

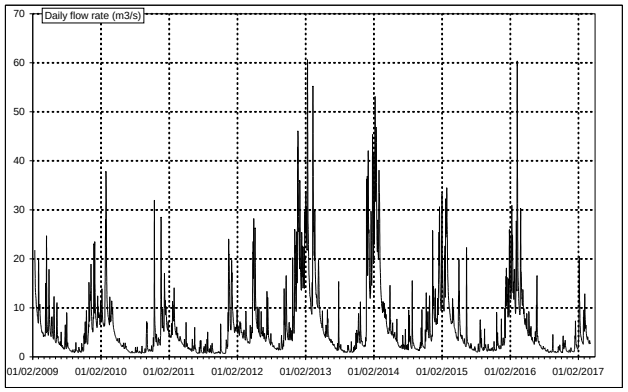

Figure 11. Water discharge of the River Couesnon between 01/02/2009 and 01/02/2017.

Regarding the sediment budgets covering the period 2009-2017, we deem that two types of actions have affected the calculated amounts. Firstly, the water releases from the new dam on the Couesnon strengthened ebb flow in a zone around the Mont. The efficiency of the releases was low from 2009 to 2013 but has been optimal since. Secondly, the excavation and erosion of the channels between the dam and the monument (and also the release of part of the sediment dredged from the storage area behind the dam) produced a sediment influx into the bay. The total sediment volume brought into the bay is estimated at about 1 Mm^3, concentrated mainly in the period 2013-2016. This volume is not negligible, but too small to account for the observed changes in the sediment budget of the study area.

CONCLUSIONS

Topographic maps and sediment budgets in the shallow inner sector of the megatidal Mont-Saint-Michel Bay have been established from the analysis of data from 15 LiDAR surveys between September 2002 and May 2017. LiDAR is a very suitable technique for investigating tidal-basin morphodynamic processes, especially because only a small part of the inner bay is subaqueous at low-water spring tides.

Morphodynamic processes in the study area produce large changes over very short periods, in comparison to other tidal basins. This makes the bay a particularly interesting study area. These changes are primarily steered by the tide, due to the very large tidal range and the ensuing high current velocities. Earlier studies have produced strong evidence that this may explain the long-term net sedimentation of the bay (Larsonneur, 1994). The hypsometric curve of the higher intertidal area has a convex-up shape, indicative of tide-dominated sedimentation processes. For the lower intertidal area, the shape is concave-up, indicative of wave-influenced sediment transport processes.

The LiDAR surveys show that sedimentation strongly fluctuates at seasonal and annual time scales. Several causes for these seasonal and annual fluctuations have come to light,

although it has not been possible to quantify the respective contributions of these causes.

- Wave action contributes to a redistribution of sediment from the lower to the higher tidal flat areas. Wind direction also influences sediment redistribution. Sediment import into the bay is associated with NW winds, whereas export is associated with S and NE winds.

- Export of sediment is further associated with high river discharges, and import with low river discharges.

- Very rapid changes in channel configurations are observed to have taken place especially during stormy winters. Channel migration rates are a factor 10 higher than reported for other estuaries. These changes influence the sediment budget by modifying transport patterns and sedimentation areas in the bay.

The influence of engineering works aimed at creating open waters around the Mont could not be identified in the zone covered by the LiDAR images up to May 2017, but it seems to be mainly restricted to a limited zone around the Mont. However, longer topographic surveys are necessary to determine to what extent the Sée-Sélune channel movements from south of the bay northward and then with swings back southward, in a seesaw movement induced by the 18.6 y nodal cycle (Levoy et al., 2017), are affected by these works.

ACKNOWLEDGMENTS

This work was partly supported by the Syndicat Mixte Mont-Saint-Michel in the acquisition of LiDAR data. Our special thanks to Romain Desguée for his help. This study was also supported by CNRS-INSU and the four French regions: Basse-Normandie, Haute-Normandie, Picardie and Nord-Pas-de-Calais. The authors would like to thank the CLAREC team for conducting the LiDAR surveys, especially Patrice Bretel, for preparing the data, and IFREMER (Institut Français de Recherche pour l'Exploitation de la Mer) and the TOTAL Foundation for the 2002 LiDAR data. Thanks to Météo-France for the wind data from modelling, and especially to Olivier Cantat of the Geophen laboratory for his help in obtaining these data. We finally thank Guillaume Izabel for his help in finalizing Figure 1b.

LITERATURE CITED

Anderson, F.E.; Black, L.; Watling, L.E.; Mook, W., and Mayer L.M., 1981. A temporal and spatial study of mudflat erosion and deposition. *Journal of Sedimentary Research*, 51(3), 729-736.

Anthony, E.J., 2009. Shore Processes and their Palaeoenvironmental Applications. *Developments in Marine Geology*, vol. 4. Elsevier Science, Amsterdam, 519 pp.

Anthony, E.J. and Dobroniak, C., 2000. Erosion and recycling of estuary-mouth dunes in a rapidly infilling macrotidal estuary, the Authie, Picardy, northern France. *Special Publications of the Geological Society of London*, 175, 109-121.

Anthony, E.J. and Orford, J., 2002. Between wave- and tide-dominated coasts: The middle ground revisited. *Journal of Coastal Research, Special Issue*, 36, 8-15.

Bearman, J.A.; Friedrichs, C.T.; Jaffe, B.E., and Foxgrover, A.C., 2010. Spatial trends in tidal flat shape and associated environmental parameters in South San Francisco Bay. *Journal of Coastal Research*, 26, 342-349.

Billeaud, I.; Tessier, B.; Lesueur, P., and Caline, B., 2007. Preservation potential of highstand coastal sedimentary bodies in a macrotidal basin: example from the Bay of Mont-Saint-Michel, NW France. *Sedimentary Geology*, 202, 754-775.

Blott, S.J.; Pye, K.; Van der Wal, D., and Neal, A., 2006. Long-term morphological change and its causes in the Mersey Estuary, NW England. *Geomorphology*, 81, 185-206.

Bonnot-Courtois C., and Levasseur, J.E., 2000. *Rétablissement du Caractère Maritime du Mont Saint-Michel. Etudes en Environnement*, volume 5. Contribution à la connaissance de la dynamique des herbus. Rapport DDE/Syndicat Mixte/Univ. Rennes 1/ UMR 8586 PRODIG CNRS. 196 p.

Bonnot-Courtois, C.; Caline, B.; L'Homer, A., and Le Vot, M., 2002. La baie du Mont-Saint-Michel et l'estuaire de la Rance ; Environnements sédimentaires, aménagements et évolution récente. *Mémoire Elf-Aquitaine*, 26, 256 p.

Brasington, J.; Langham, J., and Rumsby, B., 2003. Methodological sensitivity of morphometric estimates of coarse fluvial sediment transport. *Geomorphology*, 53(3-4), 299-316.

Brock, J.C. and Purkis, S.J., 2009. The emerging role of lidar remote sensing in coastal research and resource management. *Journal of Coastal Research, Special Issue* (53), 1-5.

Chassereau, J.E.; Bell, J.M., and Torres, R., 2011. A comparison of GPS and lidar salt marsh DEMs. *Earth Surface Processes and Landforms*. Published online in Wiley Online Library DOI: 10.1002/esp.2199.

Christiansen, C.; Vølund, G.; Lund-Hansen, L.C., and Bartholdy, J., 2006. Wind influence on tidal flat sediment dynamics: Field investigations in the Ho Bugt, Danish Wadden Sea. *Marine Geology*, 235, 78-86.

Chust, G.; Galparsoro, I.; Borja, A.; Franco, J., and Uriarte, A., 2008. Coastal and estuarine habitat mapping using LiDAR height and intensity and multi-spectral imagery. *Estuarine Coastal and Shelf Science*, 78(4), 633-643.

Davidson-Arnott, R.G.D.; Van Proosdij, D.; Ollerhead, J., and Schostak, L., 2002. Hydrodynamics and sedimentation in salt marshes: examples from a macrotidal marsh, Bay of Fundy. *Geomorphology*, 48, 209-231.

Desguée, R.; Robin, N.; Gluard, L.; Monfort, O.; Anthony, E.J., and Levoy, F., 2011. Contribution of hydrodynamic conditions during shallow water stages to the sediment balance on a tidal flat: Mont-Saint-Michel bay, Normandy, France. *Estuarine, Coastal and Shelf Science*, 94, 343-354.

Détriché, S.; Susperregui, A-S.; Feunteun, E.; Lefeuvre, J-C., and Jigorel, A., 2011. Interannual (1999-2005) morphodynamic evolution of macro-tidal salt marshes in Mont-Saint-Michel bay (France). *Continental Shelf Research*, 31, 611-630.

Eamer, J., and Wlalker, I.J., 2013. Quantifying spatial and temporal trends in beach–dune volumetric changes using spatial statistics. *Geomorphology*, 191.

Finotello, A.; Lanzoni, S.; Ghinassi, M.; Marani, M.; Rinaldo, A., and D'Alpaos, A., 2018. Field migration rates of tidal meanders recapitulate fluvial morphodynamics. *Proceedings of the National Academy of Sciences of the United States of America*, vol. 115, No 7, 1463-1468. www.pnas.org/cgi/doi/10.1073/pnas.1711330115.

Friedrichs, C.T. and Aubrey, D.G., 1996. Uniform bottom shear stress and equilibrium hypsometry of intertidal flats. In: *Mixing in Estuaries and Coastal Seas, Coastal Estuarine Stud.* 50. Ed.: C. Pattiaratchi. AGU, Washington D.C.: 405-429.

Friedrichs, C.T., 2011. Tidal flat morphodynamics: a synthesis. In: B.W. Flemming and J.D. Hansom (eds.), *Treatise on Estuarine and Coastal Science: Sedimentology and Geology*. Elsevier, 137-170.

Fuller, I.C.; Large, A.R.G.; Charlton, M.E.; Heritage, G.L., and Milan, D.J., 2003. Reach-Scale Sediment Transfers: An Evaluation of Two Morphological Budgeting Approaches. *Earth Surface Processes and Landforms*, 28, 889-903.

Gluard, L., 2012. Evolution des fonds sédimentaires sous l'influence de la divagation des chenaux aux abords du Mont-Saint-Michel. PhD, University of Caen. 300 p.

Gopfert, J. and Heipke, C., 2006. Assessment of LIDAR DTM in coastal vegetated areas. *International Archives of Photogrammetry, Remote Sensing, and Spatial Information Sciences*, 36(3), 79-85.

Gratiot, N.; Gardel, A., and Anthony, E.J, 2007. Trade-wind waves and mud dynamics on the French Guiana coast, South America: input from ERA-40 wave data and field investigations. *Marine Geology*, 236, 15-26.

Green, M. and Coco, G., 2007. Sediment transport on an estuarine intertidal flat: measurements and conceptual model of waves, rainfall and exchanges with a tidal creek. *Estuarine Coastal Shelf Science*, 72 (4), 553-569.

Héquette, A.; Hemdane, Y., and Anthony, E.J., 2008. Sediment transport under wave and current combined flows on a tide-dominated shoreface, northern coast of France. *Marine Geology*, 249, 226-242.

Heritage, G.L.; Milan, D.J.; Large, A.R.G., and Fuller, I.C., 2009. Influence of survey strategy and interpolation model on DEM quality. *Geomorphology*, 112 (3-4), 334-344.

Hooshyar, M.; Kim, S.; Wang, D., and Medeiros, S.C., 2015. Wet channel network extraction by integrating LiDAR intensity and elevation data. *Water Resources Research*, 51, 10029-10046

Janssen-Stelder, B., 2000. The effect of different hydrodynamic conditions on the morphodynamics of a tidal mudflat in the DutchWadden Sea. *Continental Shelf Research*, 20, 1461-1478.

Kim, B.O., 2003. Tidal modulation of storm waves on a macrotidal flat in the Yellow Sea. *Estuarine, Coastal and Shelf Science*, 57, 411-420.

Kirby, R., 2000. Practical implications of tidal flat shape. *Continental Shelf Research*, 20, 1061-1077.

Kirby, J.A., and Kirby, R., 2008. Medium time scale stability of tidal mud flats in Bridgwater Bay, Bristol Channel, UK: influence of tides, waves and climate. *Continental Shelf Research*, 28, 2615-2629.

Kolker, A.S.; Goodbred Jr, S.L.; Hameed, S., and Cochran, J.K., 2009. High-resolution records of the response of coastal wetland systems to long-term and short-term sea-level variability. *Estuarine, Coastal and Shelf Science*, 84, 493-508.

Lane, S.N.; Westaway, R.M., and Hicks, D.M., 2003. Estimation of erosion and deposition volumes in a large, gravel-bed, braided river using synoptic remote sensing. *Earth Surface Processes and Landforms*, 28(3), 249-271.

Larsonneur, C., 1989. La baie du Mont-Saint-Michel : un modèle de sédimentation en zone tempérée. *Bulletin de l'Institut Géologique du Bassin d'Aquitaine*, 46, 5-64.

Larsonneur, C., 1994. The Bay of Mont-Saint-Michel: a sedimentation model in a temperate macrotidal environment. *Senckenbergiana Maritima*, 24 (1/6), 3-63.

Lee, H.J.; Jo, H.R.; Chu, Y.S., and Bahk, K.S., 2004. Sediment transport on macrotidal flats in Garolim Bay, west coast of Korea: significance of wind waves and asymmetry of tidal currents. *Continental Shelf Research*, 24, 821-832.

Levoy, F.; Anthony, E.J.; Dronkers, J.; Monfort, O.; Izabel, G., and Larsonneur, C., 2017. Influence of the 18.6-year lunar nodal tidal cycle on tidal flats: Mont-Saint-Michel Bay, France. *Marine Geology*, 387, 108-113.

Levoy, F.; Anthony, E.; Monfort, O., and Larsonneur, C., 2000. The morphodynamics of megatidal beaches in Normandy, France. *Marine Geology*, 171, 39-59.

Levoy, F.; Anthony, E.J.; Monfort, O.; Robin, N., and Bretel, P., 2013. Formation and migration of transverse bars along a tidal sandy coast deduced from multi-temporal Lidar datasets. *Marine Geology*, 342, 39-52.

Levoy, F.; Garestier, F.; Froideval, L.; Monfort, O., and Poullain, E., 2016. Contribution of airborne topographic LiDAR to the study of coastal system. In *Land Surface Remote Sensing in Urban and Coastal Areas*. Elsevier BV. 231-268.

L'Homer, A.; Courbouleix, S.; Chantraine, J.; Deroin, J.P.; Bonnot-Courtois, C.; Caline, B.; Ehrhold, A.; Lautridou, J.P., and Morzadec-Kerfourn, M.T., 1999. *La Baie du Mont-Saint-Michel*. Carte géologique à 1/50 000 et notice explicative. BRGM, France, p. 100.

Liu, H., 2009. Shoreline Mapping and Coastal Change Studies Using Remote Sensing Imagery and LIDAR Data. In: *Remote Sensing and Geospatial Technologies for Coastal Ecosystem Assessment and Management*, edited by Xiaojun Yang, Springer. pp. 297-322.

Malvarez, G.C.; Cooper, J.A.G., and Jackson, D.W.T., 2001. Relationships between wave-induced currents and sediment grain size on a sandy tidal-flat. *Journal of Sedimentary Research*, 71, 705-712.

Mason, D.C.; Gurney, C., and Kennett, M., 2000. Beach topography mapping – a comparison of techniques. *Journal of Coastal Conservation*, 6, 113-124

Mason, D.C.; Scott, T.R., and Dance, S. L., 2010. Remote sensing of intertidal morphological change in Morecambe Bay, U.K., between 1991 and 2007. *Estuarine, Coastal and Shelf Science*, 87, 487-496.

Masselink, G.; Castelle, B.; Scott, T.; Dodet, G.; Suanez, S.; Jackson, D., and Floc'h, F., 2016. Extreme wave activity during 2013/2014 winter and morphological impacts along the Atlantic coast of Europe. *Geophysical Research Letters*, 43, 2135-2143.

Mehta, A.J., 2002. Mudshore dynamics and controls. In: Healy, T.; Wang, Y., and Healy, J.A. (eds.), *Muddy Coasts of the World: Processes, Deposits and Function*. Amsterdam: Elsevier Science, 19-60.

Migniot, C., 1997. *Mission Mont Saint Michel, Rétablissement du Caractère Maritime du Mont Saint-Michel, Synthèse*

Générale des Connaissances sur les Problèmes Hydro-sédimentaires. DDE Manche, 89 pp.

Moore, R.D.; Wolf, J.; Souza, A.J., and Flint, S.S., 2009. Morphological evolution of the Dee Estuary, eastern Irish Sea, UK: a tidal asymmetry approach. *Geomorphology*, 103, 588-596.

Neumeier, U., and Amos, C.L., 2006. The influence of vegetation on turbulence and flow velocities in European salt-marshes. *Sedimentology*, 53, 259-277.

Pe'eri, S. and Long, B., 2011. LIDAR technology applied in coastal studies and management. In: Pe'eri, S., and Long, B. (eds.), Applied LIDAR Techniques. *Journal of Coastal Research, Special Issue* No. 62, 1-5.

Pethick, J.S., 1996. The geomorphology of mudflats. In: Nordstrom, K.R., and Roman, C.T. (Eds.), *Estuarine Shores: Evolution, Environments and Human Alterations*. Wiley, Chichester, 185-211.

Ralston, D. and Stacey, M.T., 2007. Tidal and meteorological forcing of sediment transport in tributary mudflat channels. *Continental Shelf Research*, 27, 1510-1527.

Reineck, H.E., 1967. Layered sediments of tidal-flats, beaches and shelf bottoms of the North Sea. In: Lauff, G.H. (Ed.), Estuaries 83. *American Association for the Advancement of Science*, Washington, 191-206.

RIVAGES-GRESARC, 1996. *Rétablissement du Caractère Maritime du Mont-Saint-Michel. Etudes Hydrosédimentaires en Nature, Mesures Complémentaires. Phase 2 : Mesures sur le Terrain et Analyses des Prélèvements*. DDE de la Manche - Mission Mont-Saint-Michel. 255 p.

RIVAGES-GRESARC, 1998. *Rétablissement du Caractère Maritime du Mont-Saint-Michel. Etudes Hydrosédimentaires en Nature, Mesures Complémentaires. Phase 4 : Exploitation des Données Courantologiques et Sédimentologiques et Bilans Sédimentaires*. DDE de la Manche - Mission Mont-Saint-Michel. 122 p.

Ryu, J.H.; Kim, C.H.; Lee, Y.K.; Won, J.S.; Chun, S.S., and Lee, S., 2008. Detecting the intertidal morphologic change using satellite data. *Estuarine, Coastal and Shelf Science*, 78, 623-632.

Sallenger, A.H.; Krabill, W.B.; Swift, R.N.; Brock, J.; List, J.; Hansen, M.; Holman, R.A.; Manizade, S.; Sontag, J.; Meredith, A.; Morgan, K.; Yunkel, J.K.; Frederick, E.B., and Stockdon, H., 2003. Evaluation of airborne topographic lidar for quantifying beach changes. *Journal of Coastal Research*, 19(1), 125-133

Saye, S.E.; van der Wal, D.; Pye, K., and Blott, S.J., 2005. Beach-dune morphological relationships and erosion/accretion: an investigation at five sites in England and Wales using LIDAR data. *Geomorphology*, 72, 128-55. doi.org/10.1016/j.geomorph.2005.05.007.

Schmid, K.A.; Hadley, B.C., and Wijekoon, N., 2011. Vertical accuracy and use of topographic LIDAR data in coastal marshes. *Journal of Coastal Research*, 27(6A), 116-132.

Stevenson, J.C.; Ward, L.G., and Kearney, M.S., 1988. Sediment transport and trapping in marsh systems: implications of tidal flux studies. *Marine Geology*, 80, 37-59.

Tessier, B., 1998. Tidal cycles: annual versus semi-lunar records. In: Alexander, C.; Davis, R.A., and Henry, V.J. (Eds.), Tidalites: Processes and Products. *SEPM: Society for Sedimentary Geology, SEPM Special Publication 61*, 69-74.

Tessier, B.; Billeaud, I., and Lesueur, P., 2006. The Bay of Mont-Saint-Michel northeastern littoral: an illustrative case of coastal sedimentary body evolution and stratigraphic organization in a transgressive/highstand context. *Bulletin de la Société Géologique de France*, 177 (2), 71-78.

Thorin, S.; Radureau, A.; Feunteun, E., and Lefeuvre, J.C.; 2001. Preliminary results on a high east-west gradient in the macrozoobenthic community structure of the macrotidal Mont Saint-Michel bay. *Continental Shelf Research*, 21, 2167-2183.

Turner, R.E.; Swenson, E.M., and Milan, C.S., 2000. Organic and inorganic contributions to vertical accretion in salt marsh sediments. In: Weinstein, M.P., and Kreeger, D.A. (Eds.), *Concepts and Controversies in Tidal Marsh Ecology*. Kluwer Academic Publishing, Dordrecht, The Netherlands, 583-597.

Van der Wal, D.; Pye, K., and Neal, A., 2002. Long-term morphological change in the Ribble Estuary, northwest England. *Marine Geology*, 189, 249-266.

Van Ledden, M.; Van Kesteren, W.G.M., and Winterwerp, J.C., 2004. A conceptual framework for the erosion behaviour of sand-mud mixtures. *Continental Shelf Research*, 24, 1-11.

Weill, P.; Tessier, B.; Mouazé, D.; Bonnot-Courtois, C., and Norgeot, C., 2012. Shelly cheniers on a macrotidal flat (Mont-Saint-Michel bay, France) - Internal architecture revealed by ground-penetrating radar. *Sedimentary Geology*, 279, 173-186.

Wheaton, J.M.; Brasington, J.; Darby, S.E., and Sear, D.A., 2010. Accounting for uncertainty in DEMs from repeat topographic surveys: improved sediment budgets. *Earth Surface Processes and Landforms*, 35, 136-156.

Yang, S.L.; Ding, P.X., and Chen, S.L., 2001. Changes in progradation rate of the tidal flats at the mouth of the Changjiang (Yangtze) River, China. *Geomorphology*, 38, 167-180.

Yang, S.L.; Li, P.; Gao, A.; Zhang, J.; Zhang, W.X., and Li, M., 2007. Cyclical variability of suspended sediment concentration over a low-energy tidal flat in Jiaozhou Bay, China: effect of shoaling on wave impact. *Geo-Marine Letter*s, 27, 345-353.

Zhang, K.; Whitman, D.; Leatherman, S., and Robertson, W., 2005. Quantification of Beach Changes Caused by Hurricane Floyd Along Florida's Atlantic Coast Using Airborne Laser Surveys. *Journal of Coastal Research*, 21, n°1, 123-134.

Zimmerman, J.T.F., 1973. The influence of the subaqueous profile on wave-induced bottom stress. *Netherlands Journal of Sea Research*, 6, 542-549.